Electronic Supplementary Information

Visible Light-driven CO_2 Reduction with a Ru Polypyridyl Complex Bearing an *N*-Heterocyclic Carbene Moiety

Taito Watanabe,[a] Yutaka Saga,*[ab] Kento Kosugi,[a] Hikaru Iwami,[a] Mio Kondo [abc] and Shigeyuki Masaoka *[ab]

a.Department of Applied Chemistry, Graduate School of Engineering Osaka University, 2-1 Yamadaoka, Suita Osaka 565-0871, Japan.E-mail: mio@chem.eng.osaka-u.ac.jp, masaoka@chem.eng.osaka-u.ac.jp
b.Innovative Catalysis Science Division, Institute for Open and Transdisciplinary Research Initiatives (ICS-OTRI), Osaka University, Suita, Osaka 565-0871, Japan
c.PRESTO, Japan Science and Technology Agency (JST), 4-1-4 Honcho, Kawaguchi, Saitama 332-0012, Japan

Contents

1. Synthesis

General procedure

$NaNO_3$, KOH, NH_4PF_6, aqueous solutions of HNO_3, triethylamine, ethylene glycol, diethyl ether (Et_2O), acetonitrile-d_3 (CD_3CN) and dimethylsulfoxide-d_6 (DMSO-d_6) were purchased from FUJIFILM Wako Pure Chemical Corporation. 1-methylimidazole, 2-picolylchloride hydrochloride, methyl iodide, $NaBH_4$, tetrabutylammonium perchlorate (TBAP) and tetraethylammonium perchlorate (TEAP) were purchased from Tokyo Chemical Industry Co., Ltd. 2,2‘:6,2“-terpyridine was purchased from Aldrich. $NaHCO_3$, $NaBPh_4$, ethanol (EtOH), methanol (MeOH), ethyl acetate, chloroform (CH_3Cl) and acetonitrile (MeCN) were purchased from Kanto Chemical Co., Inc. $RuCl_3 \cdot 3H_2O$ was purchased from Tanaka Ki Kinzoku. 2-phenylbenzimidazole was purchased from Combi-Blocks. All the reagents were of highest quality available and were used as received except for TBAP and acetonitrile. TBAP was recrystallized from ethanol/H_2O. TEAP was recrystallized from MeCN/EtOH and hexane. MeCN was purified by column chromatography. H_2O was purified using a Millipore MilliQ purifier. ^1H NMR spectra were collected at room temperature on a JEOL JNM-ECZS400YH spectrometer. ESI TOF-MS spectra were collected on a JEOL JMS-T100LC mass spectrometer.

Synthesis of 1,3-dimethyl-2-phenyl-2,3-dihydro-1H-benzo[d]imidazole (BIH)

1,3-dimethyl-2-phenyl-2,3-dihydro-1H-benzo[d]imidazole (BIH) was prepared in a similar procedure described in the literature.[S1] To a solution of 2-phenylbenzimidazole (5.00 g, 25.7 mmol) and potassium hydroxide (1.54 g, 38.6 mmol) in acetone (220 mL) was added methyl iodide (1.9 mL, 30.8 mmol), and the mixture was heated at 50 ºC for overnight. Acetone was removed by evaporation and the resulting oil-like mixture was dissolved in ethyl acetate (70 mL) and H_2O (200 mL). Products were extracted three times, dried over sodium sulfate and filtered. The organic layer was directly used for the second methylation step without any purification. To the solution, methyl iodide (2.4 mL, 38.9 mmol) was added, and the mixture was heated at 80 ºC for overnight. The resulting precipitate was collected by filtration, washed with ethyl acetate to afford fine yellow solid (1,3-dimethyl-2-phenylbenzimidazolium iodide). The solid was dissolved in methanol (180 mL) and cooled in an ice bath for 5 minutes, then $NaBH_4$ (4.90 g, 129 mmol) was added portion-wise. After 30 min of stirring at room temperature, the white solid was formed, which was collected by filtration and washed with water. The crude mixture was purified by recrystallization from ethanol/water (5/1) to give 1,3-dimethyl-2-phenyl-2,3-dihydro-1H-benzo[d]imidazole (BIH) as white solid in 55 % yield for 3 steps (3.18 g, 14.2 mmol). ^{1}H NMR (400 MHz, DMSO-d_6): δ = 7.56 (2H, dd, *J* = 6.4, 1.9 Hz), 7.46 (3H, dd, *J* = 5.4, 1.9 Hz), 6.63 (2H, dd, *J* = 5.4, 3.3 Hz), 6.47 (2H, dd, *J* = 5.4, 3.2 Hz), 4.88 (1H, s), 2.49 (6H, s).

Synthesis of **RuP**$(PF_6)_2 \cdot 1.5H_2O$

RuP$(PF_6)_2 \cdot 1.5H_2O$ was prepared in a procedure previously reported by our group.[S2]

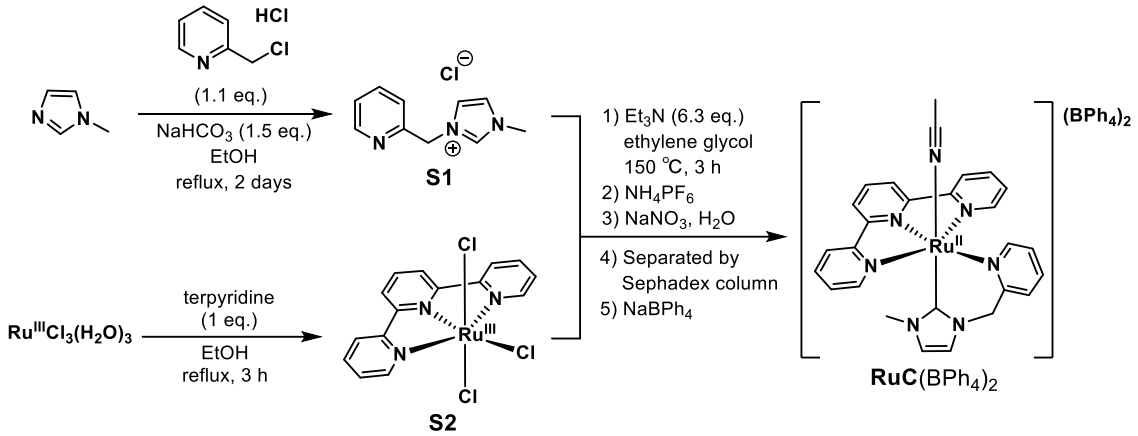

Scheme S1. Synthesis of **RuC**$(BPh_4)_2$.

Synthesis of **S1** (1-methyl-3-(2-picolinyl)-1*H* imidazolium chloride)

S1 was prepared in a similar procedure described in the literature.[S3] A solution of 1-methylimidazole (1.70 g, 20.7 mmol), 2-picolylchloride hydrochloride (3.74 g, 22.8 mmol) and $NaHCO_3$ (2.61 g, 31.1 mmol) in EtOH (15 mL) was refluxed for 48 h. After 48 h of stirring, the mixture was concentrated under reduced pressure and the gummy product was resuspended in $CHCl_3$. Undissolved inorganic salts were removed by filtration and the resulting red solution was concentrated under reduced pressure. The crude mixture was purified by chromatography (active Al_2O_3-column, eluent: $CHCl_3$/MeOH =20/1) to afford **S1** as brown oil in 86% yield (3.73 g, 17.8 mmol). ^{1}H NMR (400 MHz, DMSO-d_6): δ = 9.31 (1H, s), 8.52-8.54 (1H, m), 7.87 (1H, td, *J* = 7.8, 2.0 Hz), 7.71-7.80 (2H, m), 7.49 (1H, d, *J* = 7.6 Hz), 7.37-7.41 (1H, m), 5.57 (2H, s), 3.88 (3H, s).

Synthesis of **S2** ($[Ru^{III}(trpy)Cl_3]\cdot H_2O$)

A solution of $RuC1_3\cdot 3H_2O$ (500 mg, 1.91 mmol) and 2,2':6,2''-terpyridine (446 mg, 1.91 mmol) in EtOH (240 mL) was refluxed for 3 h. After 3 h of stirring, the resulting brown powder was collected by filtration, washed with EtOH (50 mL) and Et_2O (50 mL). The obtained crude product **S2** (722 mg, 1.64 mmol) was used for the next reaction without any purification.

Synthesis of **RuC**$(BPh_4)_2 \cdot 0.5H_2O$

A solution of **S1** (709 mg, 3.38 mmol) and **S2** (1355 mg, 3.07 mmol) in ethylene glycol (54 mL) was degassed by freezed-thawed-pumed cycle for three times. To the solution, triethylamine (2.7 mL, 19.3 mmol) was added and heated at 150 ºC for 3 hours. After the addition of aqueous ammonium hexafluorophosphate, the brown solid was formed and the solid was collected by filtration, washed with water and ether. To a solution of the solid in acetone, aqueous sodium nitrate was added and stirred for 1 minute. Mixtures were concentrated under reduced pressure and then 0.1 M HNO_3 was added. Undissolved materials were removed by filtration and the filtrate was concentrated under reduced pressure. The crude product was purified by column chromatography (Sephadex LH-20, eluent: 0.1 M HNO_3) to give the red solid. The anion exchange of the product was performed by the addition of saturated aqueous sodium tetraphenylborate. The product was purified by recrystallization from MeCN/diethyl ether to afford **RuC**$(BPh_4)_2 \cdot 0.5H_2O$ as red crystal in 11% yield (406 mg, 0.339 mmol). ^{1}H NMR (400 MHz, CD_3CN): δ = 9.08-9.12 (1H, m), 8.23-8.28 (4H, m), 8.01-8.08 (4H, m), 7.95 (2H, td, *J* = 8.0, 2.0 Hz), 7.76 (1H, d, *J* = 7.6 Hz), 7.56-7.61 (1H, m), 7.35-7.40 (2H, m), 7.14-7.21 (16H, m), 6.98 (1H, d, *J* = 1.6 Hz), 6.90 (16H, t, *J* = 7.6 Hz), 6.74 (8H, t, *J* = 7.2 Hz), 6.51 (1H, d, *J* = 2.0 Hz), 5.32 (2H, s), 2.28 (3H, s); ^{13}C NMR (400 MHz, CD_3CN): δ = 176.10, 165.41, 164.92, 164.43, 163.93, 160.05, 159.60, 158.09, 157.31, 154.74, 139.24, 138.89, 136.58, 136.27, 128.49, 127.18, 126.51, 126.49, 126.46, 126.43, 125.08, 124.71, 123.73, 123.22, 122.64, 54.70, 36.18. MS (ESI) m/z 274.57 $(M)^{2+}$; Anal. Found: C, 75.41; H, 5.41; N, 8.34. Calcd for $C_{75}H_{66}B_2N_7O_{0.5}Ru_1$: C, 75.31; H, 5.56; N, 8.20.

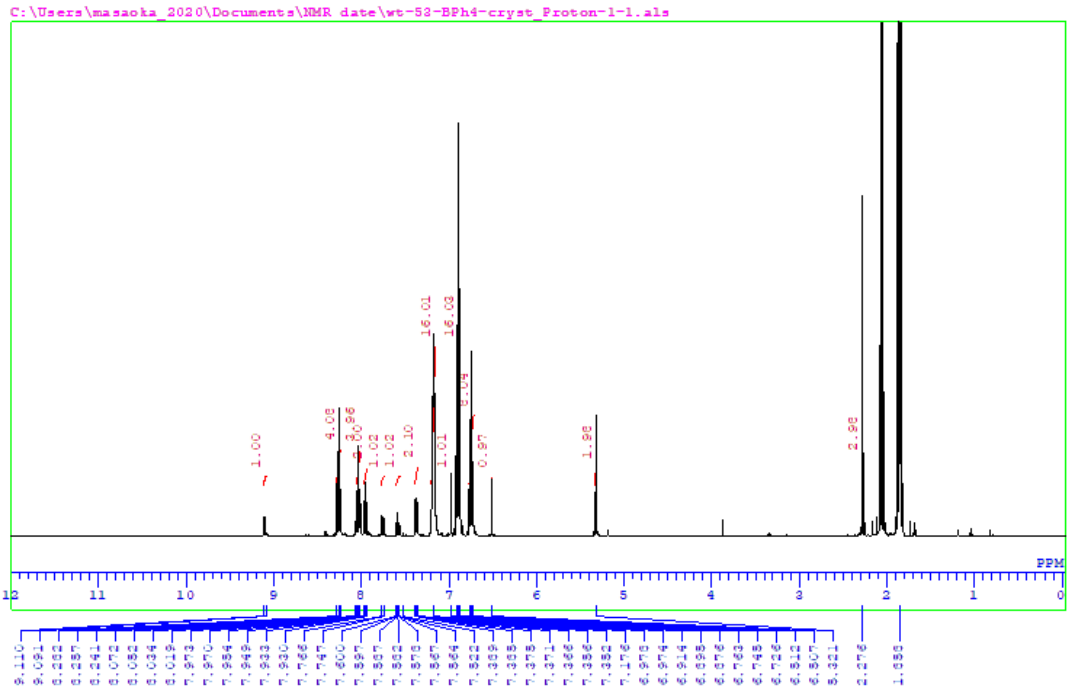

Fig. S1 ^{1}H NMR spectrum of **RuC**$(BPh_4)_2$ in CD_3CN.

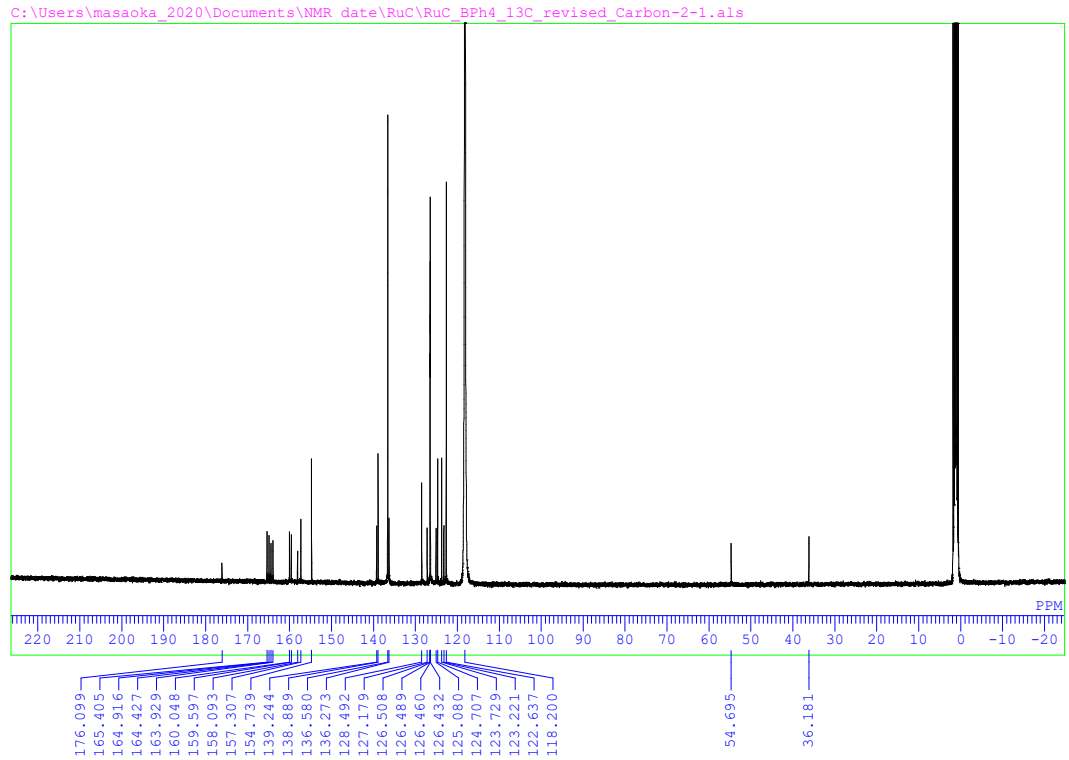

Fig. S2 ^{13}C NMR spectrum of **RuC**$(BPh_4)_2$ in CD_3CN.

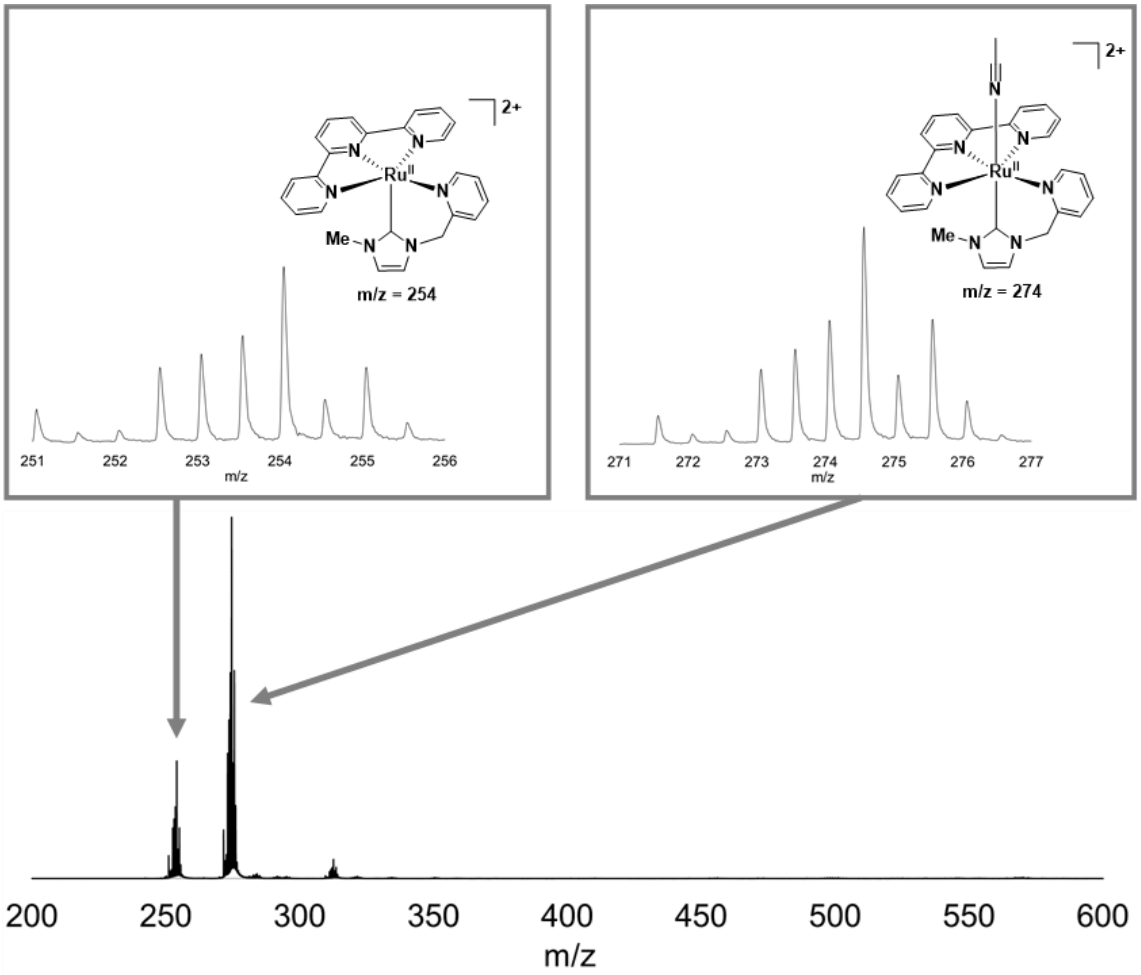

Fig. S3 An ESI-TOF mass spectrum of **RuC**$(BPh_4)_2$.

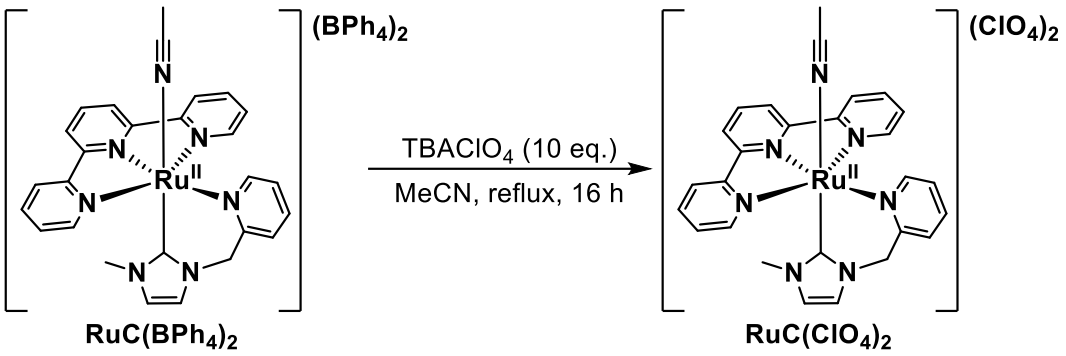

Scheme S2. Synthesis of **RuC**$(ClO_4)_2$.

Synthesis of **RuC**$(ClO_4)_2$

To a solution of **RuC**$(BPh_4)_2$ (20 mg, 0.017 mmol) in MeCN (5 mL), TBAP (57 mg, 0.17 mmol) was added, and the mixture was heated at 80 ºC for 16 hours. MeCN was removed by evaporation and the resulting solid mixture was washed by Et_2O to remove soluble inorganic salts. The solid was collected by filtration and the product was purified by recrystallization from MeCN/Et_2O to afford **RuC**$(ClO_4)_2$ as red crystal in 80% yield (10 mg, 0.013 mmol). ^{1}H NMR (400 MHz, CD_3CN): δ = 9.19-9.22 (1H, m), 8.35-8.40 (4H, m), 8.11-8.17 (4H, m), 8.05 (2H, td, *J* = 7.8, 2.0 Hz), 7.86 (1H, d, *J* = 8.0 Hz), 7.66-7.70 (1H, m), 7.45-7.49 (2H, m), 7.08 (1H, d, *J* = 2.4 Hz), 6.61 (1H, d, *J* = 2.4 Hz), 5.42 (2H, s), 2.37 (3H, s); MS (ESI) m/z 274.57 $(M)^{2+}$. HRMS (ESI): m/z calcd for $C_{27}H_{25}N_7Ru$ $[M]^{2+}$ 549.1215. Found 549.1209

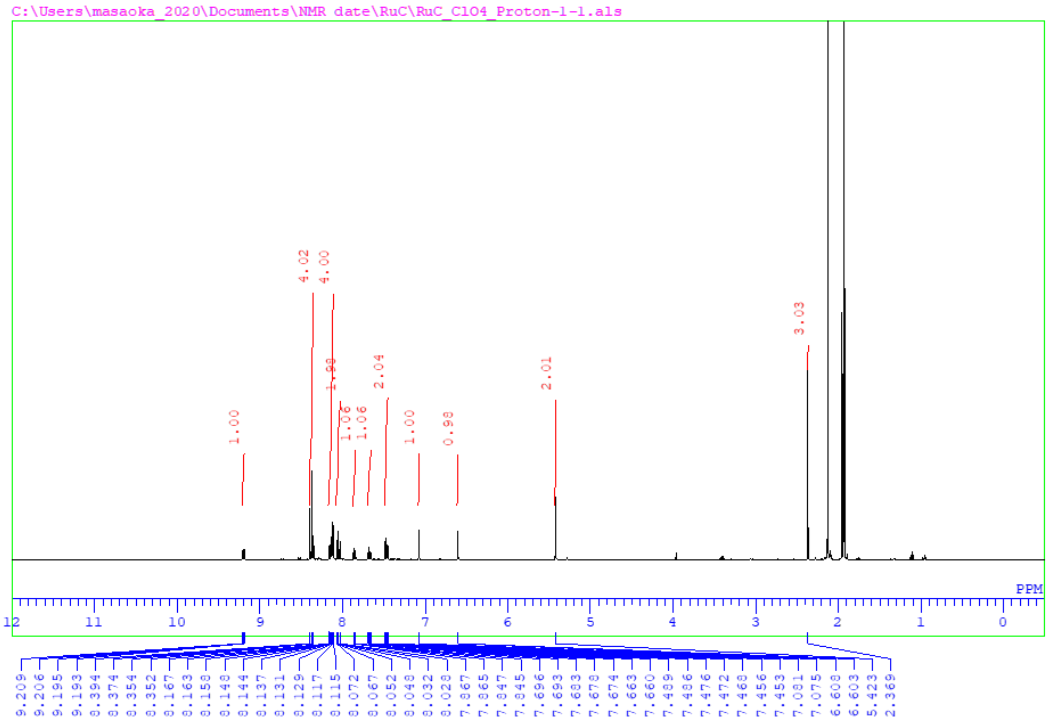

Fig. S4 ^{1}H NMR spectrum of **RuC**$(ClO_4)_2$ in CD_3CN.

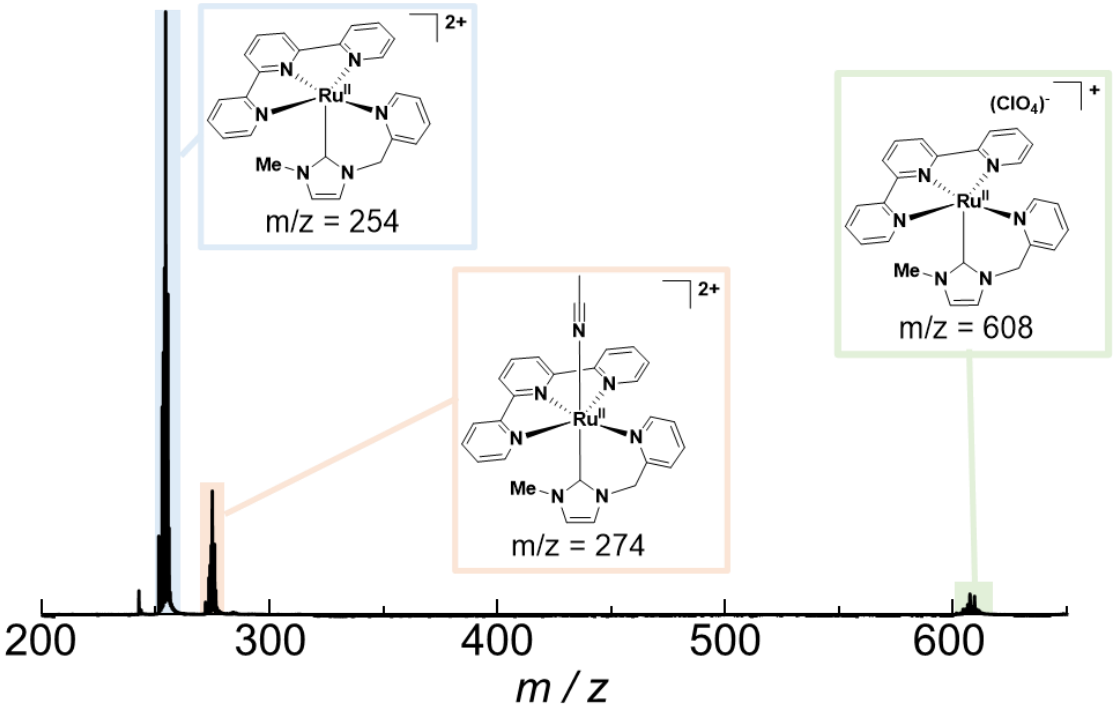

Fig. S5 An ESI-TOF mass spectrum of **RuC**$(ClO_4)_2$.

2. X-ray crystallography

Single crystal X-ray diffraction data were collected on a Synergy Custom system CCD Plate equipped with confocal monochromated Mo-Kα radiation (λ = 0.71069 Å) coated with Paratone-N (Hampton Research Corp., Aliso Viejo, CA, USA). Data was processed using CrysAlisPro system software.[S4] The structures ware solved by dual-space algorithm using SHELXT program[S5] through the Olex2 interface.[S6] All non-hydrogen atoms were refined anisotropically using a least-squares method, and hydrogen atoms were fixed at calculated positions and refined using a riding model. SHELXL−2014/7 was used for structure refinement.[S7] Full-matrix least-squares refinements on F^2 based on unique reflections with unweighted and weighted agreement factors of $R = \Sigma||F_o| - |F_c||/\Sigma|F_o|$ ($I > 2.00\ \sigma(I)$) and $wR = [\Sigma w(F_o^2 - F_c^2)^2/\Sigma w(F_o^2)^2]^{1/2}$ were performed. Mercury 4.0.0 was used for visualization and analysis of the structure. Crystallographic data have been deposited with Cambridge Crystallographic Data Centre: Deposition number CCDC 2143540 for **RuC**$(BPh_4)_2$ and 2152702 for **RuC**$(ClO_4)_2$. Copies of the data can be obtained free of charge via www.ccdc.cam.ac.uk/data_request/cif.

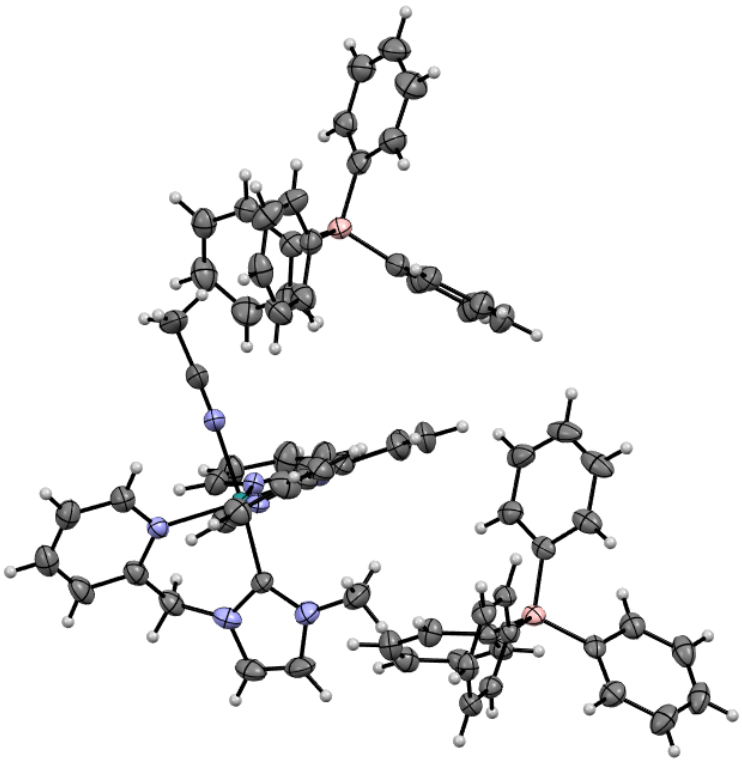

Fig. S6 An ORTEP drawing (50% probability level) of **RuC**$(BPh_4)_2$.

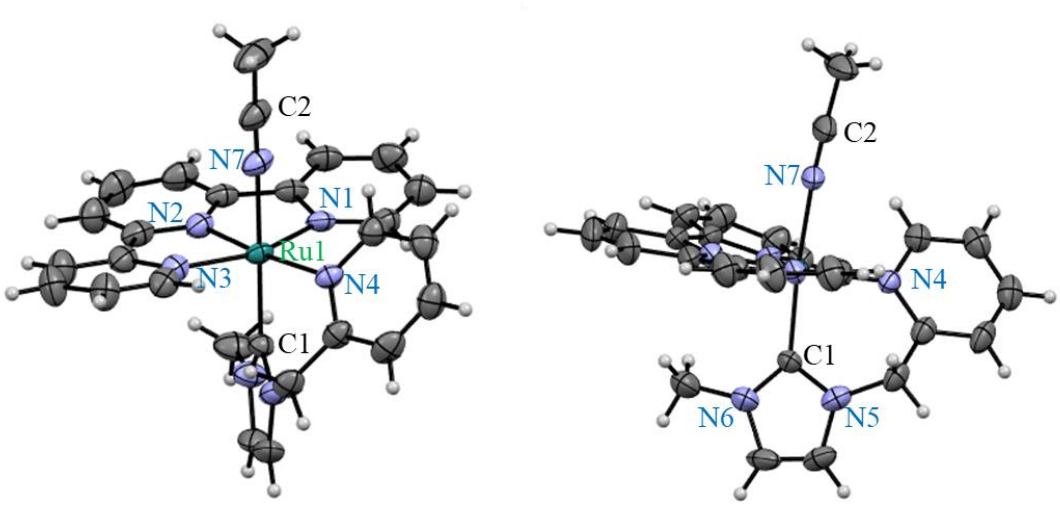

Fig. S7 ORTEP drawings (50% probability level) of cationic moiety of **RuC**$(BPh_4)_2$.

Table S1. Summary of crystallographic data for **RuC**$(BPh_4)_2$.

formula	$C_{27}\ H_{25}\ N_7\ Ru\ (C_{24}\ H_{20}\ B)_2$
crystal system	orthorhombic
space group	*Fdd2*
a / Å	40.5571 (6)
b / Å	24.8192 (4)
c / Å	24.1742 (6)
V / Å^3	24333.6 (7)
R_1	0.0546
wR_2	0.1318
GooF	1.052
Temp. / K	123

Table S2. Selected bond lengths for **RuC**$(BPh_4)_2$ and **RuP**$(PF_6)_2$.

bond	Distance / Å	Distance / Å
	RuC$(BPh_4)_2$	**RuP**$(PF_6)_2$[S2]
Ru1-N1	2.073 (4)	2.081 (5)
Ru1-N2	1.969 (4)	1.967 (5)
Ru1-N3	2.077 (4)	2.077 (5)
Ru1-N4	2.106 (4)	2.119 (5)
Ru1-N7	2.074 (4)	2.127 (5)
Ru1-C1	2.024 (4)	-
Ru1-P1	-	2.265 (2)
N7-C2	1.131 (7)	1.116 (9)
C1-N5	1.366 (6)	-
C1-N6	1.331 (6)	-

Table S3. Selected bond angles for **RuC**$(BPh_4)_2$ and **RuP**$(PF_6)_2$.

bond	Angle / degree	Angle / degree
	RuC$(BPh_4)_2$	**RuP**$(PF_6)_2$[S2]
C1-Ru1-N4	87.7 (2)	-
P1-Ru1-N4	-	83.0 (1)
N4-Ru1-N7	88.4 (2)	92.8 (2)
C1-Ru1-N7	176.1 (2)	173.1 (1)

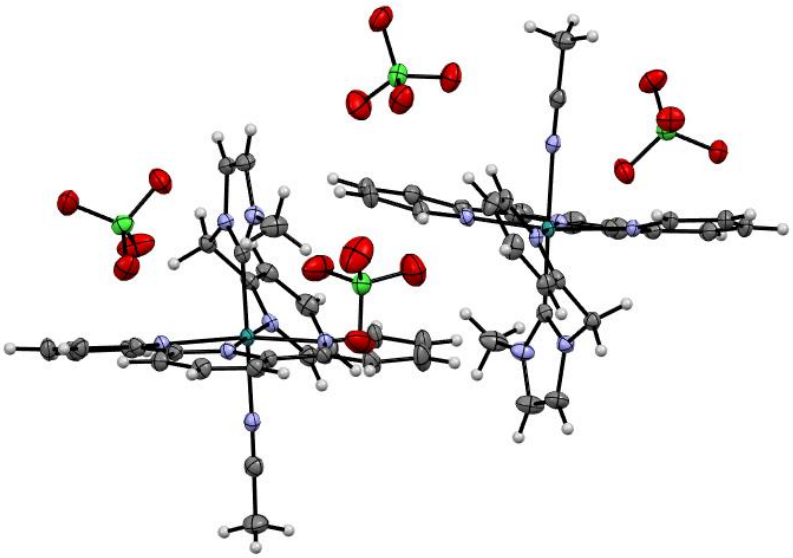

Fig. S8 An ORTEP drawing (50% probability level) of **RuC**$(ClO_4)_2$.

Table S4. Summary of crystallographic data for **RuC**$(ClO_4)_2$.

formula	$(C_{27}\ H_{25}\ N_7\ Ru)_2\ (O_4\ Cl)4$
crystal system	triclinic
space group	$P\bar{1}$
a / Å	10.6790 (2)
b / Å	12.5659 (3)
c / Å	23.1366 (5)
V / Å^3	2885.51 (11)
α / °	86.015 (2)
β / °	85.355 (2)
γ / °	68.961 (2)
R_1	0.0406
wR_2	0.1057
GooF	1.050
Temp. / K	123

3. Electrochemical measurements

Cyclic voltammetry was performed with a Bio-Logic-Science Instruments potentiostat interfaced to a computer with SP-50 software, at room temperature under Ar or CO_2 using one-compartment cell with a standard three-electrode configuration, which consisted of a glassy carbon disk (diameter 3 mm, BAS Inc.), a Ag/Ag^+ couple, and a platinum wire as the working, reference and auxiliary electrodes, respectively. The working electrode was treated between scans by means of polishing with 0.05 μm alumina paste (BAS Inc.) and washing with purified H_2O. Ferrocene was used as an internal standard, and all potentials reported within this work are referenced to the ferrocenium/ferrocene couple at 0 V. **RuC**$(BPh_4)_2$ was used for the measurement except for Fig. 2a and Fig. S9a. **RuC**$(ClO_4)_2$ was used for the measurements in Fig. 2a and Fig. S9a.

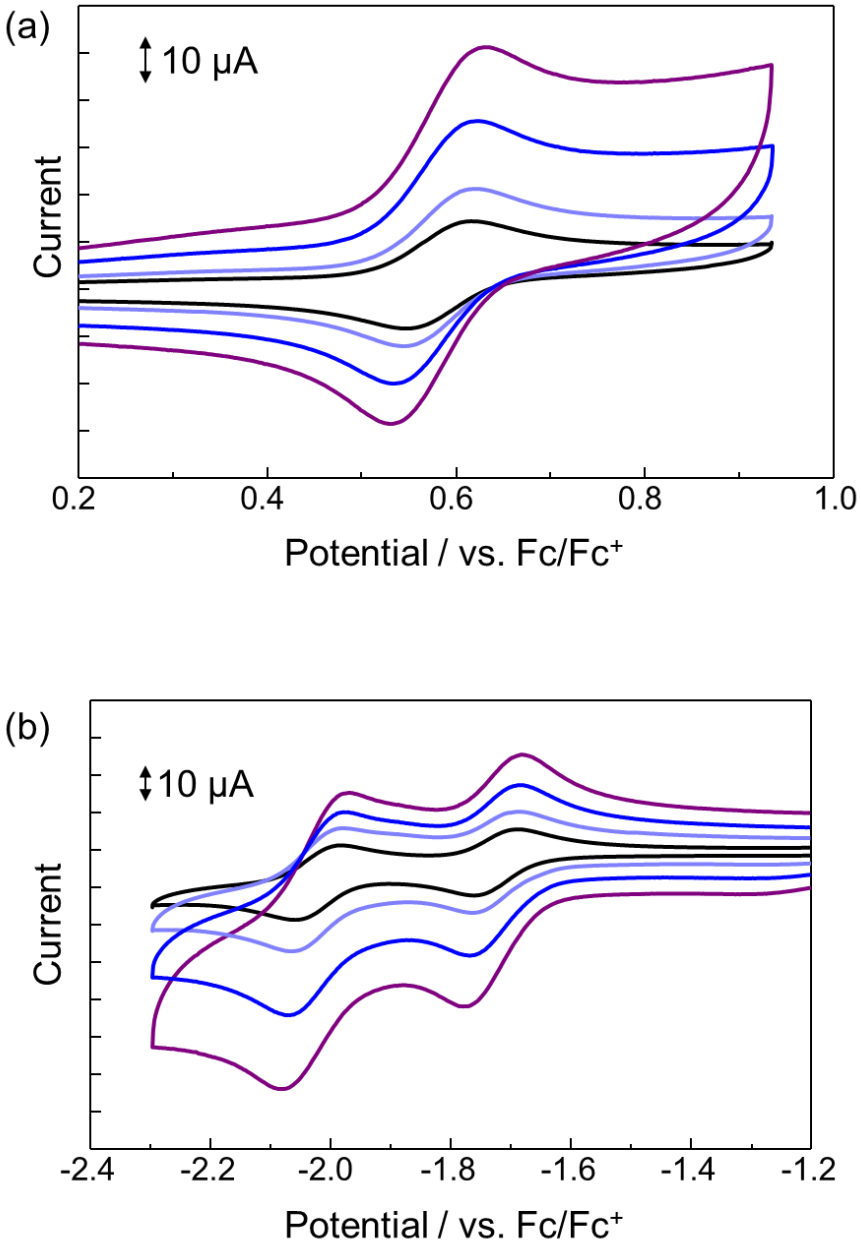

Fig. S9 CVs of **RuC** (0.5 mM) in 0.1 M TBAP/MeCN under Ar (a) in positive potential region and (b) negative potential region. Working electrode, glassy carbon; counter electrode, Pt wire; reference electrode, Ag/Ag^+; scan rate, 0.1 s^{-1} (black line), 0.2 V s^{-1} (pale blue line), 0.5 V s^{-1} (blue line) and 1.0 V s^{-1} (purple line). Potential sweeps were started from the open circuit potential for all measurements.

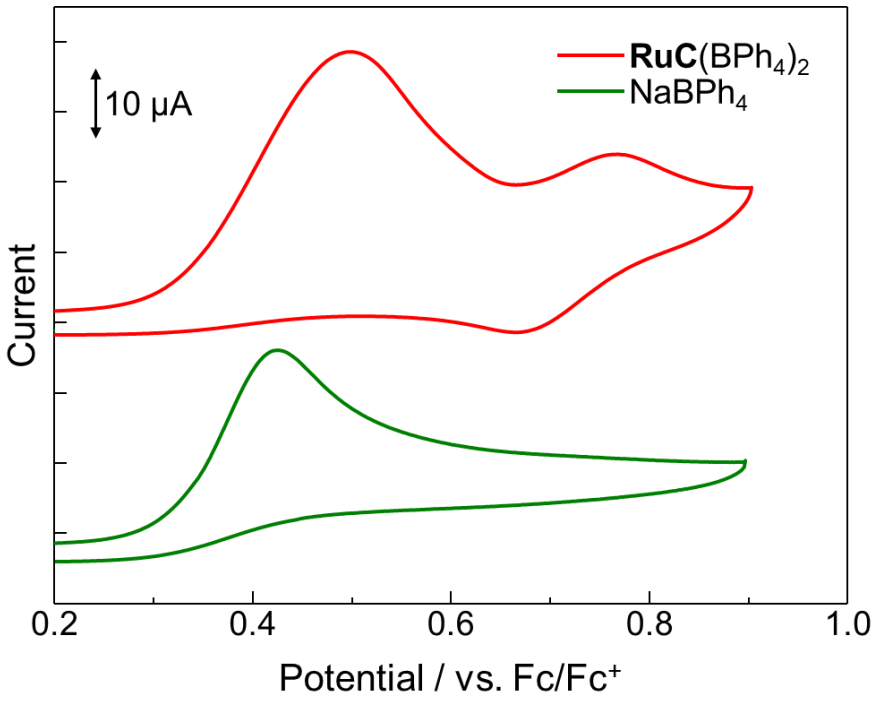

Fig. S10 CVs of **RuC**$(BPh_4)_2$ (0.5 mM, red line) and $NaBPh_4$ (0.5 mM, green line) in 0.1 M TBAP/MeCN under Ar. Working electrode, glassy carbon; counter electrode, Pt wire; reference electrode, Ag/Ag^+; scan rate, 0.1 s^{-1}. Potential sweeps were started from the open circuit potential for all measurements.

4. Spectroscopic measurements

UV-visible absorption spectra were measured on a Shimadzu UV-2450SIM spectrophotometer in MeCN at room temperature. **RuC**$(BPh_4)_2$ was used for the measurement.

5. Photocatalytic CO_2 reduction

Representative procedure for photocatalytic CO_2 reduction

A mixed solution of MeCN/H_2O (39:1, v:v) (2.0 mL) containing 20 μM **RuC**$(BPh_4)_2$ and 0.10 M BIH was purged with CO_2 for 15 minutes unless otherwise stated. The solution was then irradiated with a 150 W Xe lamp equipped with 420 nm long pass filter (Edmund Industrial Optics) to produce the light in the range of $420 \leq \lambda \leq 750$ nm at 20 ºC in a custom made aluminium box (Fig. S11) with cooling system. The amount of CO and H_2 produced at the headspace of the cell was quantified by a Shimadzu GC-8A with a TCD detector equipped with a packed column with Molecular Sieve 13X-S 60/80. Calibration curves were obtained by sampling known amounts of H_2 and CO.

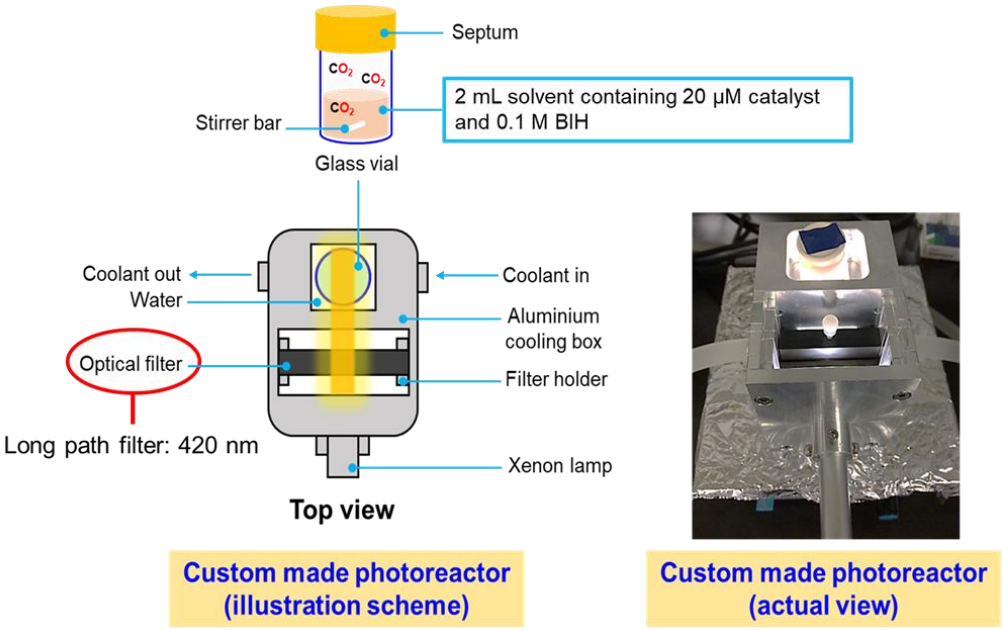

Fig. S11 Setting of a custom made photoreacter used for photocatalytic CO_2 reduction.

Stability of **RuC** for photocatalytic CO_2 reduction

In the investigation on photocatalytic activity of **RuC**, the catalysis was terminated before all BIH contained in the reaction mixture was consumed. Therefore, the decomposition of the complex is the main cause of the termination of the catalysis. Actually, when fresh BIH was added to the reaction mixture after 5 h of photolysis, the amount of evolved CO did not increase drastically (Fig. S12), indicating that **RuC** decomposes after the 5 h of photolysis.

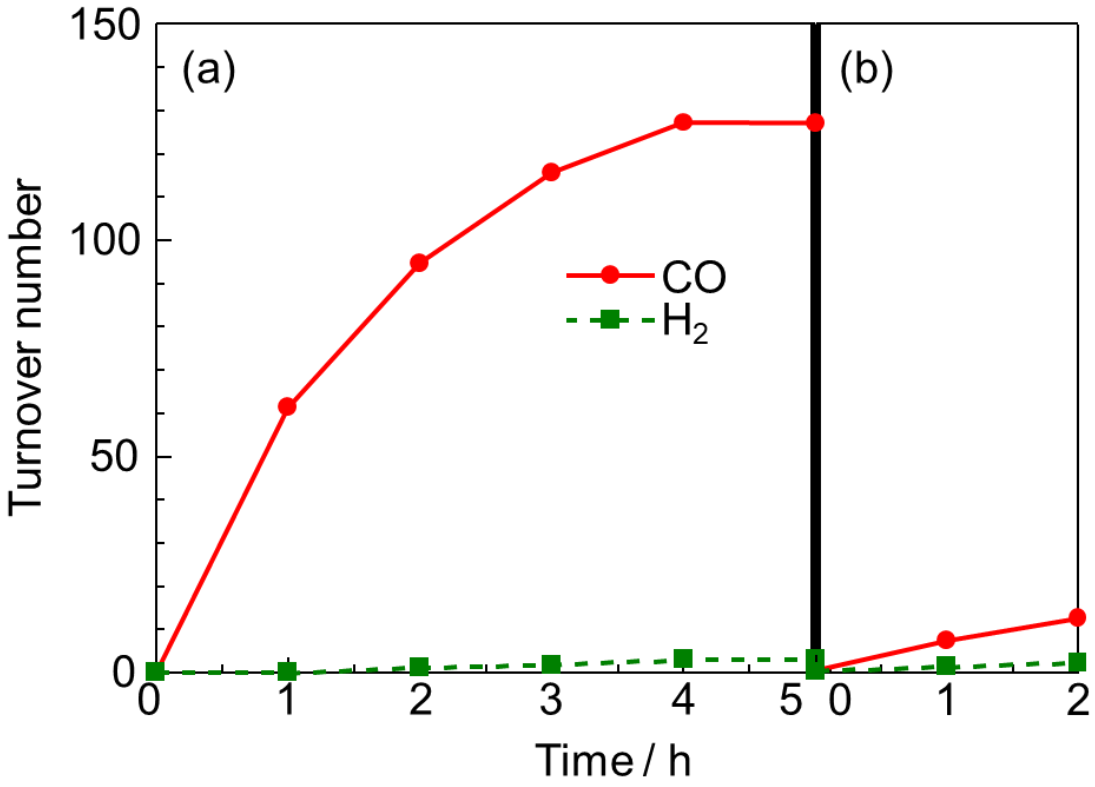

Fig. S12 (a) Turnover number of the products [CO (red) and H_2 (green)] obtained during the photocatalytic CO_2 reduction (a) with **RuC**$(BPh_4)_2$ (20 μM) and BIH (0.10 M) in CO_2-saturated-MeCN/H_2O mixture (39:1, v:v) under photoirradiation ($420 \leq \lambda \leq 750$ nm) at 20 ºC, (b) performed using the solution after 5 h reaction in (a) with the addition of BIH (0.10 M).

$^{13}CO_2$ labeling experiment

A mixed solution of MeCN/H_2O (39:1, v:v) (2.0 mL) containing 20 μM **RuC** and 0.10 M BIH was purged with Ar for 15 min, followed by $^{13}CO_2$ bubbling for 15 min. The $^{13}CO_2$ gas was produced by adding 2.0 M HCl to solid $Ba^{13}CO_3$ (98 atom% ^{13}C, Sigma Aldrich). The evolved CO was detected by a GCMS-QP2020 (Rt®-Msieve 5A (30 m, 0.53 mm ID, 50 μm df) He carrier gas, 40 ºC).

Table S5. Control experiments for the photocatalytic CO_2 reduction by **RuC**$(BPh_4)_2$ irradiated at 420 ≤ λ ≤ 750 nm for 3 h.

Entry	**RuC** (μM)	Solvent	Electron donor	TON[f]	
				CO	H_2
1	40	DMA[a]/H_2O (39:1, v:v)	BIH (0.1 M)	10.5	0.2
2	40	DMF[b]/H_2O (39:1, v:v)	BIH (0.1 M)	6.7	0.1
3	40	MeCN/TFE[c] (39:1, v:v)	BIH (0.1 M)	43.4	0.7
4	40	MeCN/TEOA[d] (4:1, v:v)	BIH (0.1 M)	13.3	0.7
5	40	MeCN/TFA[e] (39:1, v:v)	BIH (0.1 M)	0	trace

a: DMA = *N*,*N*-dimethylacetamide

b: DMF = *N*,*N*-dimethylformamide

c: TFE = 2,2,2-trifluoroethanol

d: TEOA = triethanolamine

e: TFA = trifluoroacetic acid

f: TON = turnover number

6. Quantum chemical calculation

Quantum chemical calculation were performed to evaluate the electronic structure of **RuC**, **RuC**$^{-}$, **RuC**$^{2-}$ and **RuC**$_{CO2}^{\bullet-}$. B3LYP-D3 functional[S8,S9,S10] were used to determine the optimized geometry and electronic structure. Here, LANL2DZ (with core potential) basis set was used on ruthenium, and 6-31G(*d*,*p*) basis set was used on the rest of the atoms (C, H, N and O). Solvation effects were included implicitly by the Continuum Polarized Conductor Model (CPCM), with a dielectric constant mimicking MeCN.[S11] The exited states were calculated by the time-dependent density functional theory (TD-DFT).[S12,S13,S14] All calculations were performed with the Gaussian 16 program package.[S15]

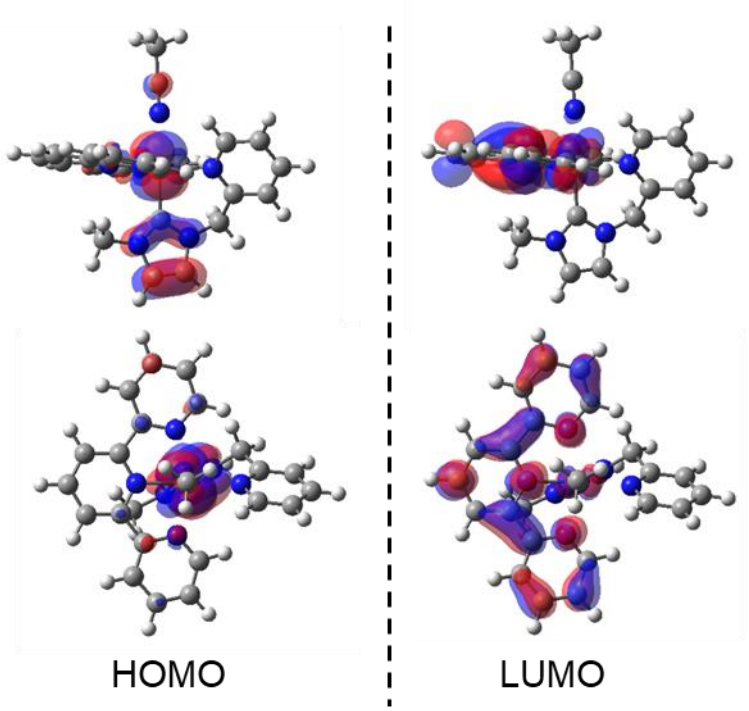

Fig. S13 Calculated molecular orbitals of **RuC**.

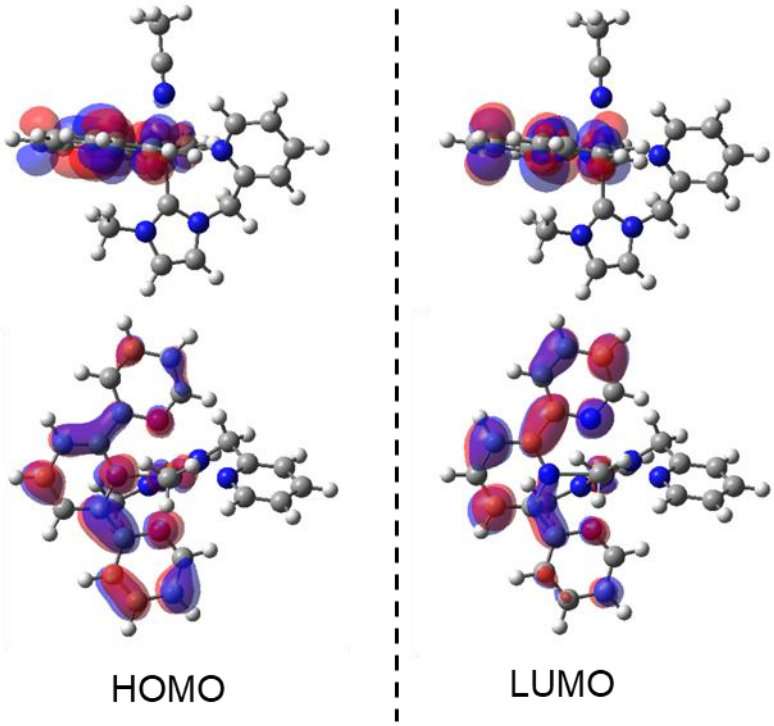

Fig. S14 Calculated molecular orbitals of **RuC**$^{-}$.

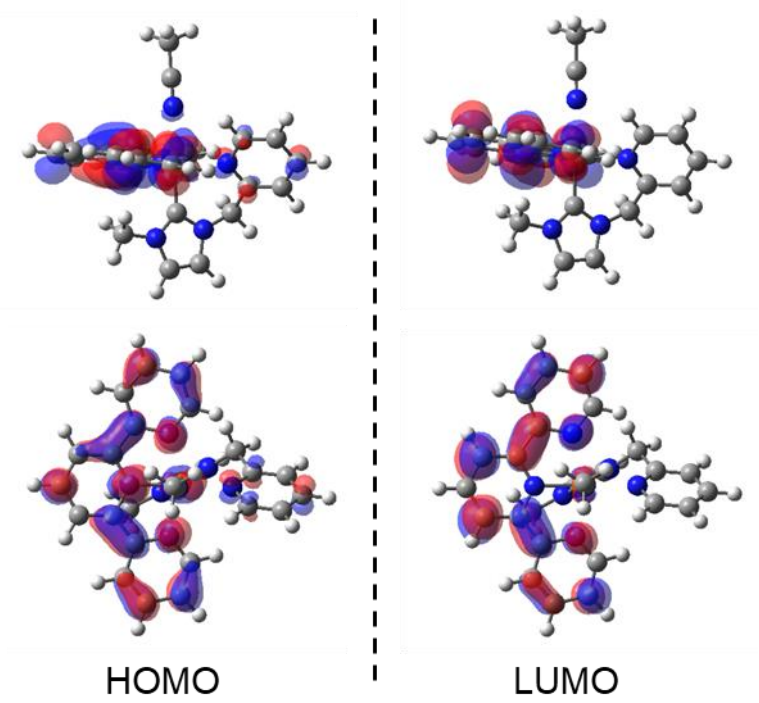

Fig. S15 Calculated molecular orbitals of **RuC**$^{2-}$.

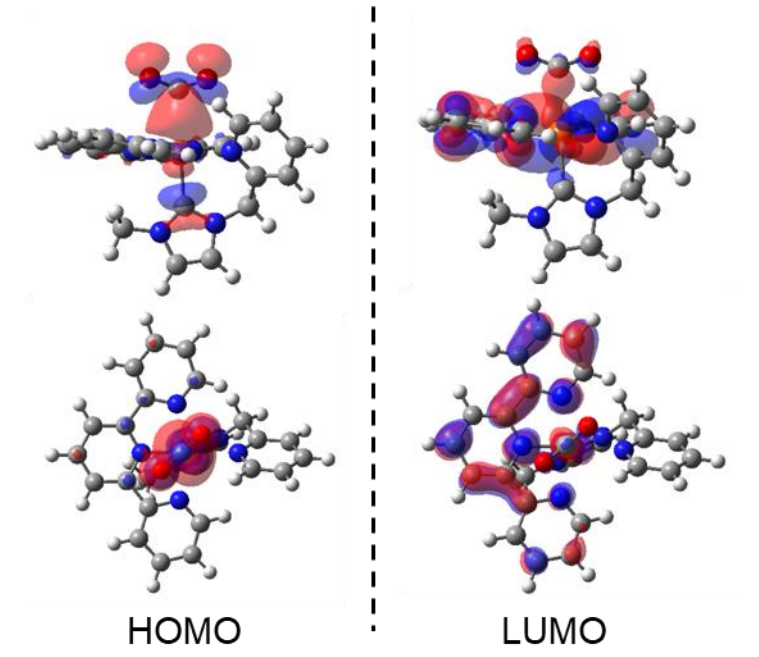

Fig. S16 Calculated molecular orbitals of **RuC**$_{CO2}^{\bullet-}$.

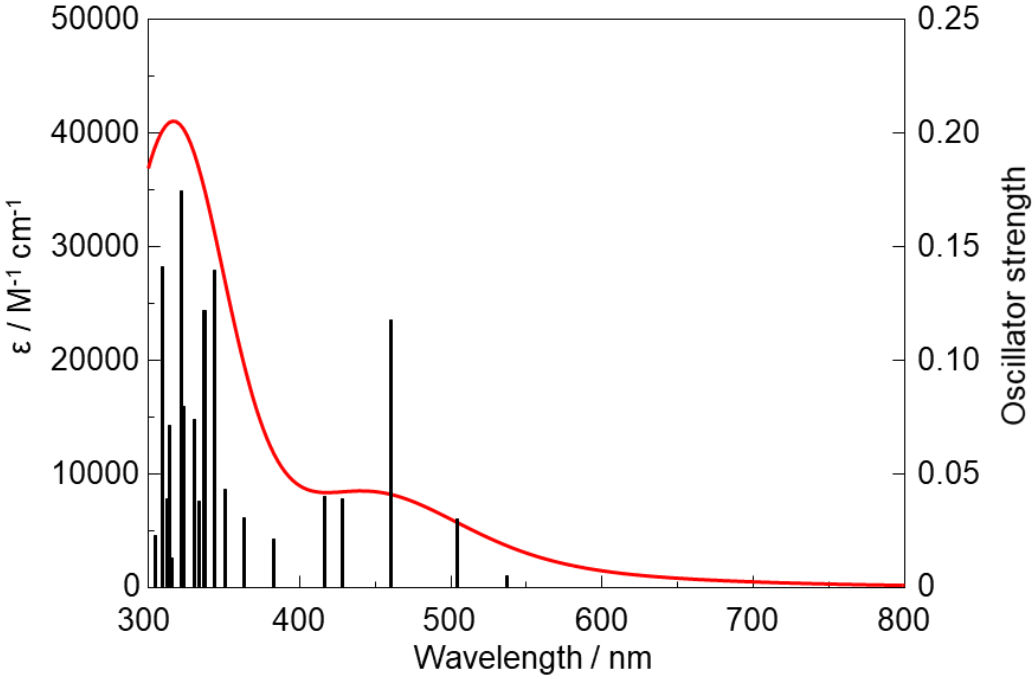

Fig. S17 Simulated absorption spectrum of **RuC** in MeCN based on TD-DFT calculations.

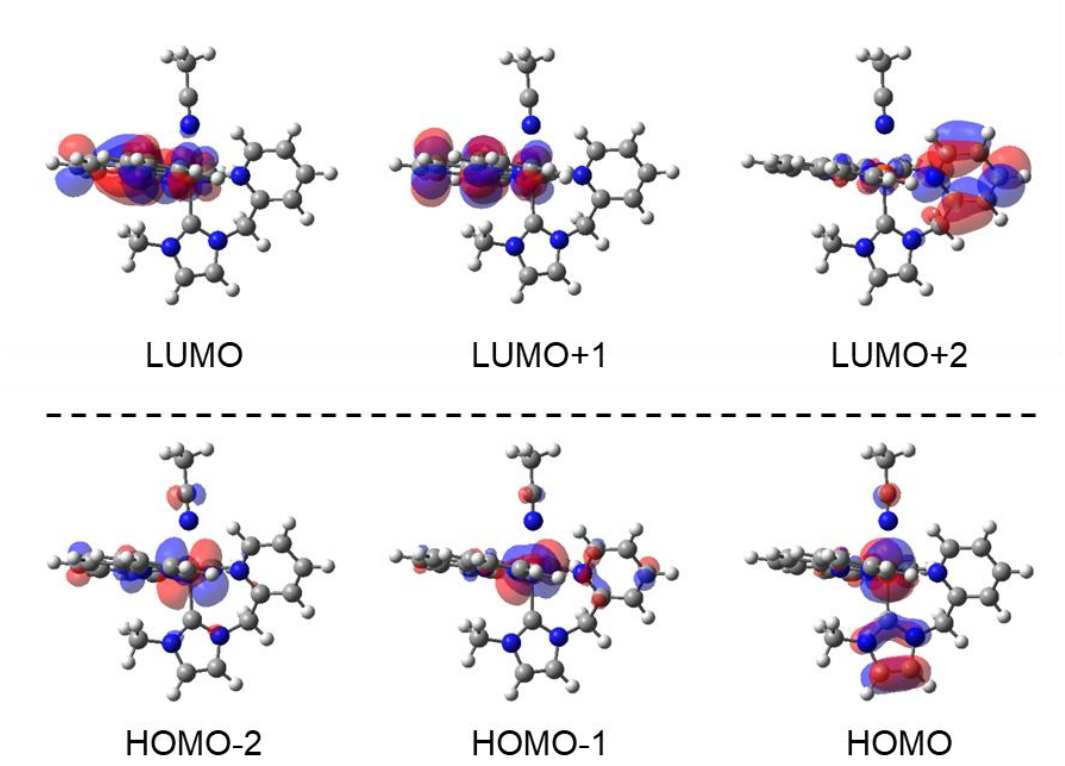

Fig. S18 Isodensity surface plots of selected frontier molecular orbitals of **RuC** based on the optimized ground-state geometry.

Table S6. Calculated TD-DFT excitation energies of **RuC** in MeCN media. *f* denotes the oscillator strength calculated for each transition.

λ / nm	*f*	Transition		
416.99	0.0398	HOMO-2	→	LUMO+1
		HOMO-1	→	LUMO+1
428.75	0.0391	HOMO-2	→	LUMO
		HOMO-2	→	LUMO+1
		HOMO-1	→	LUMO
		HOMO-1	→	LUMO+1
		HOMO	→	LUMO+1
460.99	0.1179	HOMO-2	→	LUMO
		HOMO-1	→	LUMO
		HOMO-1	→	LUMO+1
		HOMO	→	LUMO+1

7. Proposed catalytic mechanism

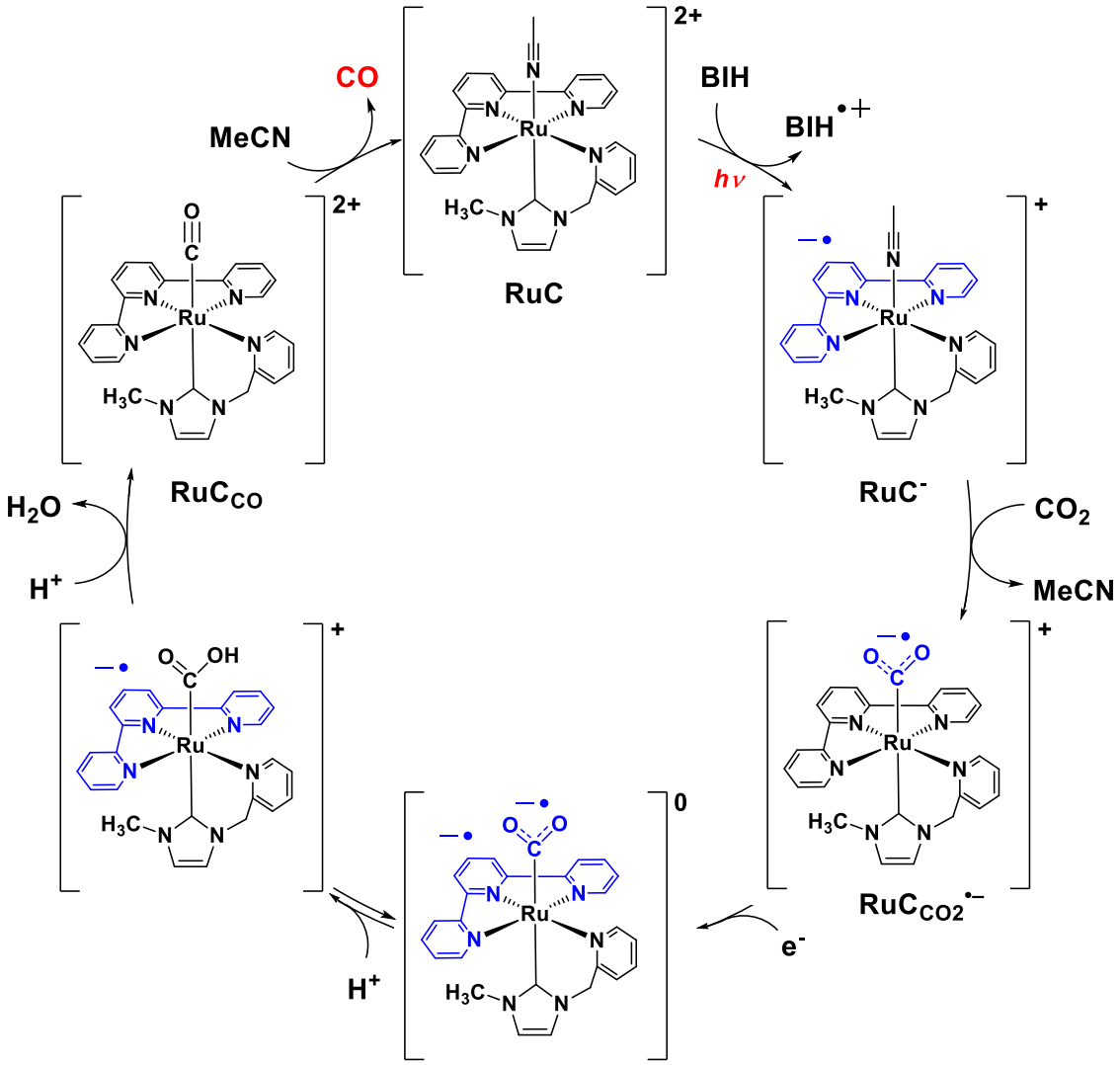

Fig. S19 Proposed catalytic mechanism for photochemical CO_2 reduction catalyzed by **RuC**.

8. Comparison of catalytic activity

Table S7. A comparison of function-integrated molecular photocatalysts for CO_2 reduction.

Catalyst (μM)	Electron donor	Light	Product	TON	[a]TOFav (h^{-1})	[b]TOFmax (h^{-1})	Ref.
RuC (*This work*)	BIH	420 ≤ λ ≤ 750 nm	CO	110 (3 h)	36.7		
RuP	BIH	420 ≤ λ ≤ 750 nm	CO	160 (11 h)	14.5		S16
RuP	TEOA	420 ≤ λ ≤ 750 nm	HCOOH	14 (4 h)	3.5		S16
$Re(bpy)(CO)_3Cl$	TEOA	λ ≥ 400 nm	CO	27 (4 h)	[c]6.8		S17
$Re(bpy)(CO)_3Br$	TEOA	λ ≥ 400 nm	CO	14 (4 h)	3.5		S18
$[Re(bpy)(CO)_3(P(OEt)_3)](SbF_6)$	TEOA	λ = 365 nm	CO	7.5 (16 h)	[c]0.45		S19
$Re(pyNHC\text{-}PhCF_3)(CO)_3Br$	BIH, TEA	solar sim.	CO	32 (4 h)	[c]8		S20
$[Re(bpy)(NS\text{-}carbene)_2(CO)_2](PF_6)$	BIH	λ ≥ 480 nm	CO	153 (15 h)	[c]10.2		S21
$[Re(bpy)_2(CO)_2](Otf)$	TEOA	λ = 405 nm	HCOOH	10 (24 h)	0.43		S22
FeTPP	TEA	cut off low UV and IR	CO	17 (10 h)	[c]1.7		S23
0CAT	TEA	cut off low UV and IR	CO	28 (10 h)	[c]2.8	7.7	S23
CAT	TEA	cut off low UV and IR	CO	30 (10 h)	[c]3.0	6.3	S23
FCAT	TEA	cut off low UV and IR	CO	23 (10 h)	[c]2.3	10.2	S23
Fe-p-TMA	BIH	λ ≥ 420 nm	CO	101 (102 h)	[c]1.0		S24
$[Ir(tpy)(ppy)Cl]^+$	TEOA	410 ≤ λ ≤ 750 nm	CO	[d]ca.80 (ca.4 h)			S25
$[Ir(tpy)(Meppy)Cl]^+$	TEOA	420 ≤ λ ≤ 750 nm	CO	[d]ca.105 (ca.4 h)			S25
$[Ir(tpy)(CF_3ppy)Cl]^+$	TEOA	420 ≤ λ ≤ 750 nm	CO	[d]ca.45 (ca.4 h)			S25
$[Ir(tpy)(Meppy)Cl](PF_6)$	TEOA	λ = 450 nm	CO	33 (ca.110 min)		35	S26
$[Ir(tpy)(Meppy)I](PF_6)$	TEOA	λ = 450 nm	CO	54		32	S26
$[(Ir(tpy)(ppy)Cl)_2\text{-}(CH_2)_2](PF_6)_2$	TEOA	λ = 450 nm	CO	81		12	S26
$[(Ir(tpy)(ppy)I)_2\text{-}(CH_2)_2](PF_6)_2$	TEOA	λ = 450 nm	CO	135		22	S26
$[(Ir(tpy)(ppy)Cl)_2\text{-}(CH_2)_8](PF_6)_2$	TEOA	λ = 450 nm	CO	92		25	S26
$[(Ir(tpy)(ppy)Cl)_2\text{-}(CH_2)_{14}](PF_6)_2$	TEOA	λ = 450 nm	CO	83		29	S26
$[(Ir(tpy)(ppy)Cl)_2\text{-}(CH_2)_2](PF_6)_2$	TEOA	λ = 450 nm	CO	41 (ca.450 min)		12	S27
$[\{(Ir(tpy)(ppy)Cl)\text{-}(CH_2)_2\}_3\text{-}Ph](PF_6)_3$	TEOA	λ = 450 nm	CO	60 (ca. 780 min)		21	S27
$N\text{-}trans\text{-}[Ir(tpy)(bpy)H](PF_6)$	TEOA	λ ≥ 410 nm	CO	[d]c.a.45 (ca.160 min)			S28
$C\text{-}trans\text{-}[Ir(tpy)(bpy)H](PF_6)$	TEOA	λ ≥ 410 nm	CO	[d]ca.45 (ca. 480 min)			S28
$C\text{-}trans[Ir(tpy)(ppy)Cl]^+$	TEOA	λ ≥ 410 nm	CO	[d]ca.50 (ca. 200 min)			S28
$[Ir(tpy)(ppy)Cl](PF_6)$	TEOA	400 ≤ λ ≤ 750 nm	CO	178±18		16±2	S29
$[Ir(tpy)(ppy)Cl](PF_6)$	TEOA	λ = 450 nm	CO	182±18		9±1	S29
$[Ir(Ph\text{-}tpy)(ppy)Cl](PF_6)$	TEOA	400 ≤ λ ≤ 750 nm	CO	262±26		16±2	S29
$[Ir(Ph\text{-}tpy)(ppy)Cl](PF_6)$	TEOA	λ = 450 nm	CO	288±29		13±1	S29
$[Ir((9\text{-}anthryl)\text{-}tpy)(ppy)Cl](PF_6)$	TEOA	400 ≤ λ ≤ 750 nm	CO	310±30		6.4±0.6	S29
$[Ir((9\text{-}anthryl)\text{-}tpy)(ppy)Cl](PF_6)$	TEOA	λ = 450 nm (2.0×10^{-8} einstein/s)	CO	344±30		4.6±0.4	S29
$[Ir((9\text{-}anthryl)\text{-}tpy)(ppy)Cl](PF_6)$	TEOA	λ = 450 nm (7.9×10^{-9} einstein/s)	CO	530±50		3.0±0.4	S29
$[Ir((4'\text{-}F\text{-}Ph)\text{-}tpy)(ppy)Cl](PF_6)$	TEOA	400 ≤ λ ≤ 750 nm	CO	248±25		10±2	S29
$[Ir(tpy)(bpy)Cl]^{2+}$	TEOA	410 ≤ λ ≤ 750 nm	CO HCOOH	2 (24 h) 20 (24 h)	[c]0.08 0.8		S30
Mes-IrPCY2	BIH	λ ≥ 400 nm	CO HCOOH	62 (24 h) 323(24 h)	[c]2.6 [c]13.5		S31
Mes-IrPCY2	BIH	λ ≥ 400 nm	HCOOH	2080 (146 h)	[c]14.3		S31
$Os(bpy)(CO)_2Cl_2$	TEOA	Osram Xe	CO	11.5 (4.5 h)	[c]2.6		S32
$Os(dmbpy)(CO)_2Cl_2$	TEOA	Osram Xe	CO	19.5 (4.5 h)	[c]4.3		S32
$Os(bpy)(CO)_2Cl_2$	TEOA	λ ≥ 326 nm	CO HCOOH	24 (14 h) 8.5 (14 h)	[c]1.7 [c]0.6		S33
$Os(dmbpy)(CO)_2Cl_2$	TEOA	λ ≥ 326 nm	CO HCOOH	45 (14 h) 15 (14 h)	[c]3.2 [c]1.1		S33
$Os(dtbbpy)(CO)_2Cl_2$	TEOA	λ ≥ 326 nm	CO HCOOH	47 (14 h) 8 (14 h)	[c]3.4 [c]0.6		S33
$Os(d(COOiPr)bpy)(CO)_2Cl_2$	TEOA	λ ≥ 326 nm	CO HCOOH	7 (14 h) 2 (14 h)	[c]0.5 [c]0.1		S33
[Ru(CNC)(bpy)(MeCN)]	BIH	solar sim.	CO	55		8.3	S34

a: The turnover frequency was calculated by dividing the turnover number with duration of photoirradiation.

b: Only the maximum turnover frequency mentioned in the articles are listed.

c: The turnover frequency calculated from the numbers in the articles are listed.

d: The approximate turnover number from the figures in the articles are listed.

9. References

S1. R. N. Sampaio, D. C. Grills, D. E. Polyansky, D. J. Szalda and E. Fujita, *J. Am. Chem. Soc*., **2020**, *142*, 2413-2428.

S2. G. Nakamura, M. Okamura, M. Yoshida, T. Suzuki, H. D. Takagi, M. Kondo and S. Masaoka, *Inorg. Chem*., **2014**, *53*, 7214-7226.

S3. S. D. Adhikary, D. Bose, P. Mitra, K. D. Saha, V. Bertolasi and J. Dinda, *New J. Chem*., **2012**, *36*, 759-767.

S4. CrysAlisPro, Oxford Diffraction Ltd., Version 1.171.39.46.

S5. G. M. Sheldrick, *Acta Cryst*. **2015**, A71, 3.

S6. O. V. Dolomanov, L. J. Bourhis, R. J. Gildea, J. A. K. Howard, H. Puschmann, *J. Appl. Crystallogr*. **2009**, *42*, 339.

S7. G. M. Sheldrick, *Acta Cryst*. 2015, A71, 3.

S8. A. D. Becke, *J. Chem. Phys*., **1993**, *98*, 5648.

S9. C. Lee, W. Yang and R. G. Parr, *Phys. Rev. B*., **1988**, *37*, 785.

S10. S. Grimme, *J. Chem. Phys*., **2006**, *124*, 034108.

S11. J. Tomasi, B. Mennucci and R. Cammi, *Chem. Rev*., **2005**, *105*, 2999.

S12. M. E. Casida, C. Jamorski, K. C. Casida, D. R. Salahub, J. Chem. Phys. 1998, 108, 4439.

S13. R. E. Statmann, G. E. J. Scuseria, Chem. Phys. 1998, 109, 8218.

S14. R. Bauernschmitt, R. Ahlrichs, Chem. Phys. Lett. 1996, 256, 454.

S15. *Gaussian 16*, Revision C.01, M. J. Frisch, G. W. Trucks, H. B. Schlegel, G. E. Scuseria, M. A. Robb, J. R. Cheeseman, G. Scalmani, V. Barone, G. A. Petersson, H. Nakatsuji, X. Li, M. Caricato, A. V. Marenich, J. Bloino, B. G. Janesko, R. Gomperts, B. Mennucci, H. P. Hratchian, J. V. Ortiz, A. F. Izmaylov, J. L. Sonnenberg, D. Williams-Young, F. Ding, F. Lipparini, F. Egidi, J. Goings, B. Peng, A. Petrone, T. Henderson, D. Ranasinghe, V. G. Zakrzewski, J. Gao, N. Rega, G. Zheng, W. Liang, M. Hada, M. Ehara, K. Toyota, R. Fukuda, J. Hasegawa, M. Ishida, T. Nakajima, Y. Honda, O. Kitao, H. Nakai, T. Vreven, K. Throssell, J. A. Montgomery, Jr., J. E. Peralta, F. Ogliaro, M. J. Bearpark, J. J. Heyd, E. N. Brothers, K. N. Kudin, V. N. Staroverov, T. A. Keith, R. Kobayashi, J. Normand, K. Raghavachari, A. P. Rendell, J. C. Burant, S. S. Iyengar, J. Tomasi, M. Cossi, J. M. Millam, M. Klene, C. Adamo, R. Cammi, J. W. Ochterski, R. L. Martin, K. Morokuma, O. Farkas, J. B. Foresman, and D. J. Fox, Gaussian, Inc., Wallingford CT, 2016.

S16. S. K. Lee, M. Kondo, M. Okamura, T. Enomoto, G. Nakamura and S. Masaoka, *J. Am. Chem. Soc*., **2018**, *140*, 16899.

S17. J. Hawecker, J.-M. Lehn and R. Ziessel, *Chem. Commun*., **1983**, *286*, 536-538.

S18. J. Hawecker, J.-M. Lehn and R. Ziessel, *Helv. Chim. Acta*, **1986**, *69*, 1990-2012.

S19. H. Hori, F. P. A. Johnson, K. Koike, O. Ishitani and T. Ibusuki, *J. Photochem. Photobiol., A*, **1996**,*96*,171-174.

S20. A. J. Huckaba, E. A. Sharpe and J. H. Delcamp, *Inorg. Chem*., **2016**, *55*, 682-690.

S21. A. Maurin, C.-O. Ng, L. Chen, T.-C. Lau, M. Robert and C.-C. Ko, *Dalton Trans.*, **2016**, *45*, 14524-14529.

S22. Y. Hameed, P. Berro, B. Gabidullin and D. Richeson, *Chem. Commun*., **2019**, *55*, 11041-11044.

S23. J. Bonin, M. Chaussemier, M. Robert and M. Routier, *ChemCatChem*, **2014**, *6*, 3200-3207.

S24. H. Rao, J. Bonin and M. Robert, *Chem. Commun*., **2017**, *53*, 2830-2833.

S25. S. Sato, T. Morikawa, T. Kajino and O. Ishitani, *Angew. Chem. Int. Ed.*. **2013**, *52*, 988-992

S26. R. O. Reithmeier, S. Meister, B. Riegar, A. Siebel, M. Tschurl, U. Heiz and E. Herdtweck, *Dalton Trans*., **2014**, *43*, 13259-13269.

S27. R. O. Reithmeier, S. Meister, A. Siebel and B. Rieger, *Dalton Trans*., **2015**, *44*, 6466-6472.

S28. K. Garg, Y. Matsubara, M. Z. Ertem, A. Lewandowska-Andralojc, S. Sato, D. J. Szalda, J. T. Muckerman and E. Fujita, *Angew. Chem. Int. Ed*., **2015**, *54*, 14128-14132.

S29. A. Genoni, D. N. Chirdon, M. Boniolo, A. Sartorel, S. Bernhard and M. Bonchio, *ACS Catal*., **2017**, *7*, 154-160.

S30. S. Sato and T. Morikawa, *ChemPhotoChem*, **2018**, *2*, 207-212.

S31. K. Kamada, J. Jung, T. Wakabayashi, K. Sekizawa, S. Sato, T. Morikawa, S. Fukuzumi and S. Saito, *J. Am. Chem. Soc*., **2020**, *142*, 10261-10266.

S32. J. Chauvin, F. Lafolet, S. Chardon-Noblat, A. Deronzier, M. Jakonen and M. Haukka, *Chem. Eur. J*., **2011**, *17*, 4313-4322.

S33. C. E. Castillo, J. Armstrong, E. Laurila, L. Oresmaa, M. Haukka, J. Chauvin, S. Chardon-Noblat and A. Deronzier, *ChemCatChem*, **2016**, *8*, 2667-2677.

S34. S. Das, R. R. Rodrigues, R. W. Lamb, F. Qu, E. Reinheimer, C. M. Boudreaux, C. E. Webster, J. H. Delcamp and E. T. Papish, *Inorg. Chem*., **2019**, *58*, 8012-8020.